

This work was written as part of one of the author's official duties as an Employee of the United States Government and is therefore a work of the United States Government. In accordance with 17 U.S.C. 105, no copyright protection is available for such works under U.S. Law.

Public Domain Mark 1.0

<https://creativecommons.org/publicdomain/mark/1.0/>

Access to this work was provided by the University of Maryland, Baltimore County (UMBC) ScholarWorks@UMBC digital repository on the Maryland Shared Open Access (MD-SOAR) platform.

Please provide feedback

Please support the ScholarWorks@UMBC repository by emailing scholarworks-group@umbc.edu and telling us what having access to this work means to you and why it's important to you. Thank you.

RESEARCH ARTICLE | JUNE 16 2014

100 eV electron temperatures in the Maryland centrifugal experiment observed using electron Bernstein emission

R. R. Reid; C. A. Romero-Talamás; W. C. Young; R. F. Ellis; A. B. Hassam

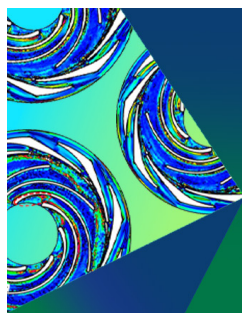


Phys. Plasmas 21, 063305 (2014)

<https://doi.org/10.1063/1.4883499>



CrossMark



Physics of Plasmas Physics of Fluids

Special Topic: Coherent Vortical
Structures in Fluids and Plasmas

Submit Today!



100 eV electron temperatures in the Maryland centrifugal experiment observed using electron Bernstein emission

R. R. Reid,^{1,a)} C. A. Romero-Talamás,² W. C. Young,³ R. F. Ellis,⁴ and A. B. Hassam⁴

¹*U.S. Naval Research Laboratory, Washington, DC 20375, USA*

²*Department of Engineering, University of Maryland Baltimore County, Baltimore, Maryland 21250, USA*

³*CPLA, University of Wisconsin, Madison, Wisconsin 53706, USA*

⁴*IREAP, University of Maryland, College Park, Maryland 20742, USA*

(Received 17 February 2014; accepted 13 May 2014; published online 16 June 2014)

Thermal electron Bernstein emission has been observed at the second harmonic of the electron cyclotron frequency at the mid-plane of the Maryland Centrifugal eXperiment. The emission is received in the X-mode polarization and coupled to the Bernstein wave by the B-X mode conversion process. The average B-X coupling efficiency is approximately 20%. The observed emission indicates thermal electron temperatures an excess of 100 eV in the core of the rotating plasma. The measured electron temperature is consistent with recent ion temperature measurements and indicates that the total energy confinement time exceeds 500 μ s. © 2014 AIP Publishing LLC.

[<http://dx.doi.org/10.1063/1.4883499>]

I. INTRODUCTION

The Maryland centrifugal experiment (MCX) is a magnetic mirror device with a variable mirror ratio ($MR \equiv B_{max}/B_{min} = 2.0 - 24.0$). An axial high voltage electrode biased -10 kV against the vacuum vessel drives supersonic azimuthal flows via the $\mathbf{E} \times \mathbf{B}$ drift. The resulting centrifugal force acts to confine the plasma to the magnetic minimum (mid-plane) and eliminate the loss cone found in simple magnetic mirrors.¹ A further benefit of the rotation is that the sheared velocity profile acts to stabilize the interchange instability and reduce radial transport.¹⁻⁴ The central electrode is isolated from the vacuum vessel by ceramic insulators at the two magnetic maxima, which prevent the plasma from line-tying to the vessel walls and allow rotation. The outermost flux surface, which is free to rotate, is referred to as the last good flux surface (LGFS). Measuring the electron temperature inside the rotating plasma has been a persistent problem. Electrostatic probes are quickly destroyed by contact with the rotating plasma. Traditional electron cyclotron emission cannot be used to measure the electron temperature because of the high plasma density and low magnetic field $n \sim 5 \times 10^{20} \text{ m}^{-3}$ and $B \sim 0.2 \text{ T}$.³ The plasma is therefore “overdense,” ($\omega_p \gg \omega_c$), and the first few harmonics of the cyclotron frequency cannot propagate through the plasma. Thompson scattering is a robust diagnostic technique⁵ but requires lasers that are prohibitively expensive to implement. Previously, electron temperatures in MCX have been inferred using atomic line intensity ratios generated by impurity ions;⁶ however, continued improvement in vacuum conditions have reduced the impurity emissions below usable levels. In this work, we present the first direct measurements of the electron temperature in MCX, achieved using electron Bernstein emission. These measurements, combined with measurements of the ion temperature, allow us to make the first estimates of the total energy confinement time for MCX discharges.

The electron Bernstein wave (EBW) is an electrostatic mode in magnetized plasmas, which has found utility both as a temperature diagnostic and as a means of electron heating and current drive in overdense plasmas.⁷⁻⁹ Bernstein waves are useful for diagnostics in overdense plasmas because they may propagate through arbitrarily dense plasmas and easily reach blackbody emission intensities. Numerical estimates¹⁰ for the optical depth (τ) of the plasma at the mid-plane of MCX yield $\tau > 100$ for the second harmonic of the cyclotron frequency, easily satisfying the condition $\tau > 2$ needed to ensure blackbody emission. As such, EBWs are useful as a temperature diagnostic provided that the wave can be successfully coupled to an electromagnetic mode, which can then be detected by an antenna remote from the plasma and that the efficiency of this mode conversion is well known.

In this paper, we will be dealing with the B-X mode conversion process,¹¹ in which the EBW may couple to the X-mode when it encounters the upper hybrid resonance (UHR) defined by $f_{UH}^2 = f_p^2 + f_{ce}^2$. This process is highly dependent on the density length scale (L_n) at the UHR. Early measurements indicated that the density length scale normally found at the UHR in MCX is not favorable to efficient mode conversion, the conversion efficiency generally being less than 1%. Drawing on work done on CDX-U,⁹ we employ a local plasma limiter to modify the plasma density gradient directly in front of the receiving antenna to improve B-X conversion efficiency. During normal operation, the UHR is found within 0.5 cm of the vacuum vessel wall and outside of the rotating plasma. The plasma conditions in this region are sufficiently mild that implementing a ceramic limiter is straightforward and may be accomplished without disturbing the plasma rotation.

II. B-X MODE CONVERSION

The direct B-X mode conversion model describes a process by which an EBW mode converts to the electromagnetic X-mode.¹¹ The B-X-O process is another mode coupling

^{a)}Electronic mail: remington.r.reid@gmail.com

process in which the EBW excites the electromagnetic O-mode;⁷ however, as all of the radiation detected at the mid-plane has been in the X-mode, we will restrict our analysis to the B-X process. The dispersion relation for the X-mode has two cutoffs given by

$$\omega_{R,L} = \pm \frac{\omega_c}{2} + \sqrt{\frac{\omega_c^2}{2} + \omega_p^2}, \quad (1)$$

where $\omega_{R,L}$ denotes the right and left-hand cutoff frequencies and a resonance at the upper hybrid resonance (UHR). The X-mode can propagate freely above the right hand-cutoff and between the left-hand cutoff and the UHR while it is evanescent between the right-hand cutoff and the UHR as well as below the lefthand cutoff. The B-X process then proceeds as follows: in the overdense interior of the plasma, EBWs are thermally excited at harmonics of the local cyclotron frequency and propagate radially outward until they encounter the UHR layer. At the UHR, the EBWs couple to the slow X-mode, which propagates back and is reflected by the left-hand cutoff. If the density gradient near the UHR is sufficiently steep, then the right-hand cutoff will be close enough to the UHR for the slow X-mode to tunnel through the evanescent region and couple to the fast X-mode, which propagates away from the UHR and escapes the plasma. If the density gradient is too shallow, then the reflected slow wave cannot tunnel across the evanescent region and radiation is trapped inside the UHR surface. The coupling efficiency C between the EBW and the final X-mode depends on the plasma density profile the UHR and is given by¹¹

$$C = 4e^{-\pi\eta}(1 - e^{-\pi\eta})\cos^2\left(\frac{\phi}{2} + \theta\right), \quad (2)$$

$$\eta \sim \frac{\omega_c L_n}{c \alpha} \left(\sqrt{1 + \alpha^2} - 1\right)^{1/2}, \quad (3)$$

where $\alpha = (\omega_p/\omega_c)$, $L_n = n_e/(\partial n_e/\partial x)$, $\theta = \text{phase of } \Gamma(-i\eta/2)$, and ϕ is the phase difference between the slow X-mode moving toward the UHR and the reflected wave traveling back to the lefthand cutoff. All quantities are evaluated at the UHR. Physically, the righthand and lefthand cutoffs form the walls of a lossy resonant cavity pumped by mode-converting EBWs. The parameter η relates distances between the lefthand cutoff, UHR, and righthand cutoff. Transmission is maximized when the waves reflecting from both cutoffs destructively interfere ($\phi/2 + \theta = \text{any integer multiple of } \pi$).

III. EXPERIMENTAL APPARATUS

Microwave emission is collected between 8.2 and 12.4 GHz using a 13 dB pyramidal horn. This frequency band encompasses the range of second harmonic cyclotron frequencies found directly in front of the receiving horn (10.5–11.6 GHz). The horn is mounted using a rotatable flange so that different polarizations may be measured shot to shot. The horn is recessed 1 cm behind the main vessel wall to protect it from contact with the plasma. The detector

is calibrated using a solid state noise source that outputs a known radiation intensity across 8.2–12.4 GHz. The solid state source allows the entire radiometer system to be calibrated, including waveguide runs and pressure windows. The density gradient is modified by a local limiter consisting of an alumina cylinder, coaxial with the microwave horn, extended anywhere from 0 to 2.5 cm beyond the vessel wall. The UHR occurs within 0.5 cm of the vacuum vessel wall so the limiter may be extended or retracted past the UHR. Extending the limiter 0.5 cm past the vessel wall has been found to yield the highest average B-X conversion efficiency. Moving the limiter more than ± 1.0 cm from this position reduces the emission below detectable levels. An array of three electrostatic double probes⁵ measures the plasma density at three radial positions near the UHR and allow us to calculate the plasma density gradient at the UHR.

IV. MEASUREMENTS

Electron Bernstein emission via the B-X conversion process has three defining characteristics. First, the emission should only appear at harmonics of the cyclotron frequency. Second, it should be strongly polarized in the X-mode. Finally, the intensity should be a strong function of the density gradient at the UHR. As we will show, the measured emission clearly exhibits of these characteristics.

The first condition is verified by measuring the emission spectrum over an extended series of discharges. The strength of the mid-plane magnetic field may be varied and the effect on the emission spectrum observed. In all cases, microwave emission is observed only in the frequency band corresponding to the second harmonics of ω_c at mid-plane.

To quantify the degree of polarization, emission spectra in the X- and O-modes were obtained by averaging the emission received between 1.5 and 2.5 ms after the initial breakdown. This procedure was repeated across several frequencies over a series of 80 discharges with identical plasma conditions. The results are shown in Figure 1. The average intensity in the X-mode is as much as 5 times greater than the average intensity in the O-mode. The polarization of

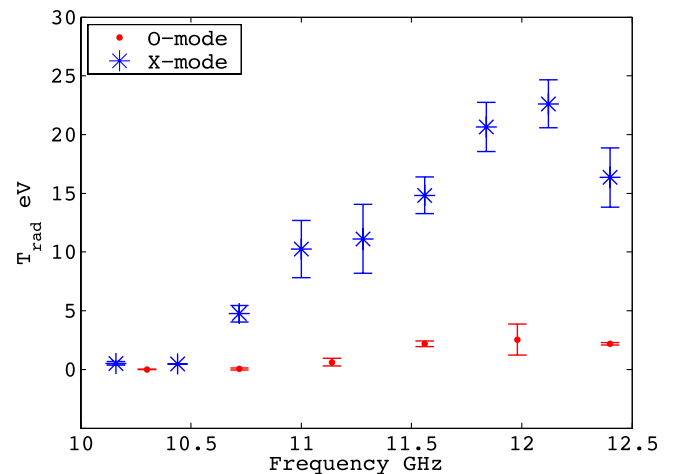


FIG. 1. Average emission polarized perpendicular (X-mode) and parallel (O-mode) to the magnetic field. Note that neither mode exhibits emission below 10.5 GHz, which is the lowest 2nd harmonic of the cyclotron frequency possible in MCX.

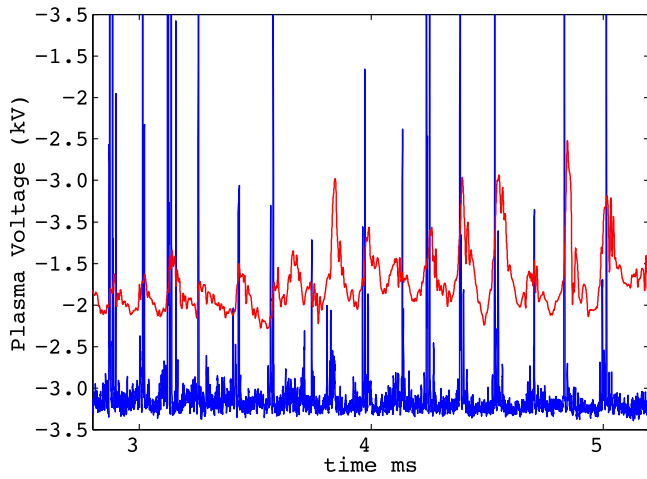


FIG. 2. Radiation detected in the X-mode at 11.56 GHz (compared with periodic crashes in the voltage across the rotating plasma. As the voltage crashes, bursts of microwave radiation are received by the antenna.

the emission also demonstrates that the signal is not contaminated by reflections from elsewhere in the experiment as multiple reflections would scramble the polarization.

Finally, the observed emission displays an extreme dependence on plasma conditions at the UHR, consistent with EBW emission. The emission measured in the X-mode from a typical discharge is shown in Figure 2. The emission occurs in periodic clusters of intense bursts. These clusters are associated with crashes in the voltage across the plasma. These voltage crashes are caused by a residual $m=2$ interchange mode which is only partially stabilized by the sheared rotation profile. The physics of this partial stabilization in MCX has been studied extensively^{12,13} and will be briefly summarized here. Initially, the sheared rotation profile is sufficient to stabilize the plasma against interchange modes. This leads to a reduction in radial density and momentum transport. As a consequence of the reduced transport, both the plasma voltage (rotation) and plasma pressure increase. Both the increased plasma pressure and the centrifugal force from the increased rotation are destabilizing to the interchange modes and eventually the shear stabilization is overwhelmed, exciting the $m=2$ mode. This leads to an increase in radial transport, reducing the pressure and slowing the rotation. The net effect is to remove the forces driving instability. Stable flow resumes and the rotation accelerates until the cycle repeats itself, leading to a quasi-periodic cycle of voltage crashes. The picture that emerges for EBW emission is as follows: during steady flow conditions the density length scale L_n is unfavorable for B-X mode conversion and little or no emission is observed. As pressure builds, the $m=2$ interchange mode is destabilized and transports plasma density radially outward. Because of the $m=2$ mode structure of the turbulence generated at the edge, regions of higher and lower density are alternately swept past the limiter and receiving antenna. As they rotate in front of the receiving horn, the higher density perturbations shorten L_n and couple the EBW to the X-mode. This yields a burst of emission before a lower density perturbation rotates into view and the emission is choked off. The characteristic emission during this phase consists of brief periods of

intense emission interspersed with equally brief periods of suppressed emission. As the rotation slows, the interchange stabilizes and the unfavorable density gradient is restored, cutting off emission entirely.

In light of this explanation for the clusters of emission bursts, we expect a strong correlation in the time between consecutive emission peaks within a single burst and the flow speed at the plasma edge (UHR). Specifically, the time between peaks should equal the half the rotation time for the plasma edge. The flow speed at the plasma edge is measured with an array magnetic probes that are spaced evenly in a ring around the inside of the vacuum chamber wall.¹⁴ The correlation between fluctuations measured by the magnetic probes is used to measure both the rotation speed and mode structure at the edge of the plasma.^{12,14} For the discharges studied in this paper, the edge rotation speed varied between 65 and 75 km/s. The plasma edge is located at a radius of 25 cm, so the expected time to complete half a rotation is about 11 μ s. Figure 3 shows a histogram of the times between emission spikes taken over several discharges with identical plasma conditions. The maximum around 11 μ s strongly supports our proposed model for the relationship between the interchange mode and the EBW emission.

Having established that the observed emission results from mode converted EBWs, we now attempt to measure the conversion efficiency and thus the electron temperature. The high flow speed at the plasma edge (~ 70 km/s) presents a challenge in measuring the density fluctuations with electrostatic probes. The time it takes for an element of plasma to flow past the limiter is ~ 1.5 μ s, which is comparable to the time response of the double probes. Noise inherent in the probe signals further obscures the density gradient measurement. However, the probes have been successful in demonstrating that the emission clusters are correlated with an increase in the average density gradient near the UHR, and in estimating the average value of density gradient. The probes measure the plasma density near the UHR. These density measurements are used to find the density gradient at

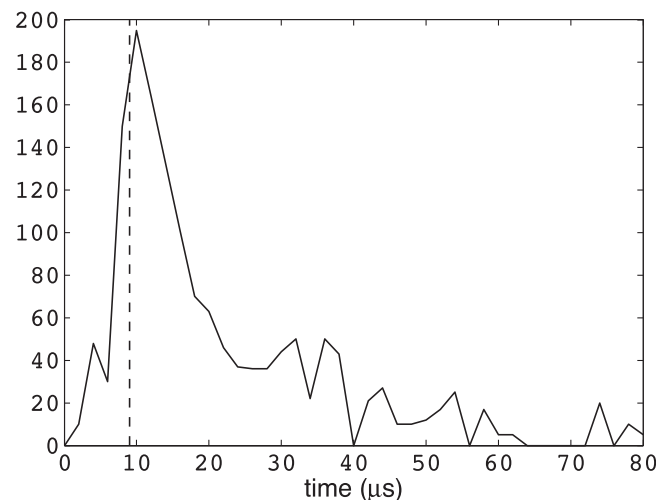


FIG. 3. Histogram showing the times between successive bursts in X-mode emission collected over 8 discharges. The dashed line at 11 μ s indicates the time expected for the interchange mode to cycle the plasma density in front of the viewing horn once.

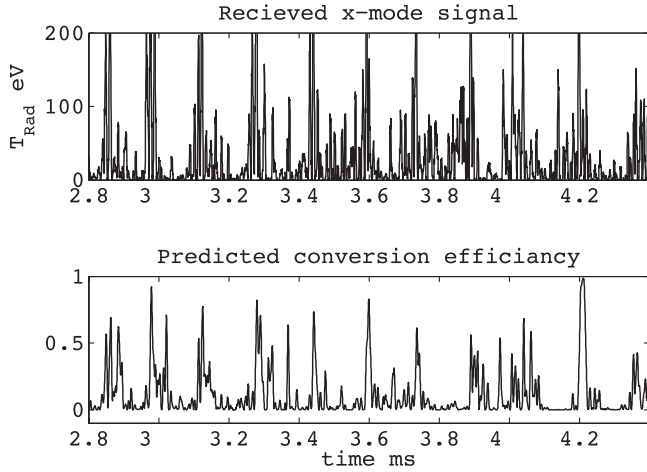


FIG. 4. Relative timing between the received x-mode signal (a) and the B-X conversion efficiency predicted using the density gradient as measured using the array of electrostatic probes (b).

the UHR, which allows us to calculate the B-X conversion efficiency using Eq. (2). The result is a measurement of the conversion efficiency as a function of time. Figure 4 shows the predicted B-X conversion efficiency based on plasma densities measured using the electrostatic probe array along with the actual measured EBW emission. Assuming a constant electron temperature the two traces should be proportional. Visually, the clusters of X-mode emission are indeed associated with higher predicted conversion efficiency. This is verified by a linear cross-correlation of the two signals as shown in Figure 5. The peak at zero lag confirms the conversion efficiency, as measured by the electrostatic probes, is indeed correlated with the X-mode emission.

The electrostatic probes indicate that the conversion efficiency fluctuates between 0 and about 70% during an interchange with an average B-X coupling efficiency of 0.20 ± 0.06 . The average radiation temperature measured during a typical discharge is around 20 eV, implying a peak electron temperature around 100 eV in the hottest part of the plasma. The average conversion efficiency of 20% is lower than efficiencies seen in other EBW experiments where efficiencies as high as 75% have been observed.^{8,9} The reason is that

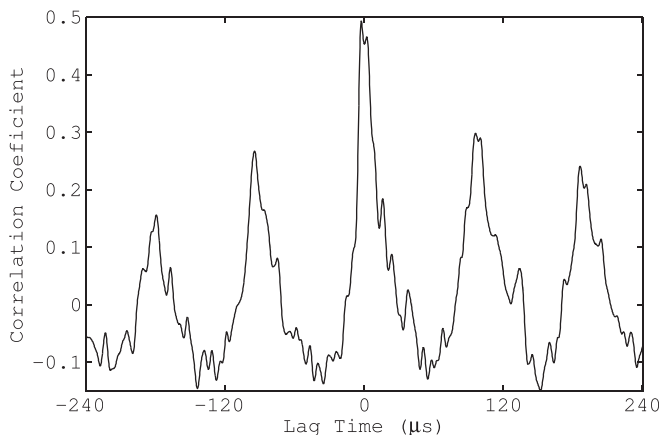


FIG. 5. Linear Cross-correlation between the X-mode radiation and the predicted conversion efficiency. The strong peak at zero lag shows the correlation between the measured signal and the predicted efficiency.

efficient conversion occurs only when turbulence at the UHR transiently produces a favorable density gradient. It may be possible to tune the radial location of the limiter to yield a higher average conversion efficiency. Experiments with extending the limiter -0.5 , 0.5 , and 1.0 cm from the usual position have all resulted in decreased emission intensities.

V. TEMPERATURE PROFILE ESTIMATION

The magnetic field at the mid-plane of the MCX device is not uniform, decreasing with radius from 0.212 T at the central electrode to 0.185 T at the vessel wall. The magnetic field strength increases axially by about 5% within the view of the receiving horn because of proximity to the mirror coils. This inhomogeneity limits the spatial resolution of the radiometer, as any detector frequency will be in resonance with several radial and axial locations. The electron temperature is not expected to vary significantly along the field lines owing to high parallel conductivity, so the emission spectrum is primarily determined by the radial electron temperature profile $T_e(r)$. Harmonic overlap is not a concern because the magnetic field decreases monotonically along any path drawn from a point within the plasma to the receiving horn.

Because of the inhomogeneity of the magnetic field, there is a saddle shaped region of plasma in resonance with the radiometer, so that the radiometer is effectively measuring some average electron temperature over the saddle shaped region. Rather than attempting to recover the radial temperature profile directly from the measured spectrum, we have prepared a numeric code, which calculates emission spectra for many possible profiles and then selects the one that best reproduces the measured results.

The code models emission in two dimensions, r and z . The mid-plane region is divided into a grid spanning $0 < r < 30$ cm and $-30 < z < 30$ cm. Electron temperature is assumed to be constant along magnetic field lines, and the magnetic field is taken to be the vacuum magnetic field.⁴ Based on an assumed electron temperature profile at mid-plane ($z=0$), the code assigns a temperature to each grid point. The temperature outside the rotating plasma is assumed to be zero. The effective antenna view is modeled as a cone with an angle that is varied from 0° to 80° . Resonant plasma is assumed to emit as a black body and to be optically thick while non-resonant plasma is assumed to be transparent. Radiation is assumed to propagate directly from the resonant plasma to the antenna. Emission spectra are calculated for all combinations of cone angles and temperature profiles and then compared to the measured emission spectrum using least squares minimization. The electron temperature profile, which yields the best fit to the measured spectrum, is shown in Figure 6 together with recent measurements made of the radial ion temperature profile.¹⁵ The corresponding cone angle was 38° . The model accurately predicts the emission spectrum over most of the observed frequency range (Fig. 7), although the measured and predicted spectra begin to diverge above 12 GHz. To check the validity of this technique, this procedure has been repeated for a range of magnetic field intensities. The magnetic field strength was varied from 90% to 110% of its normal strength

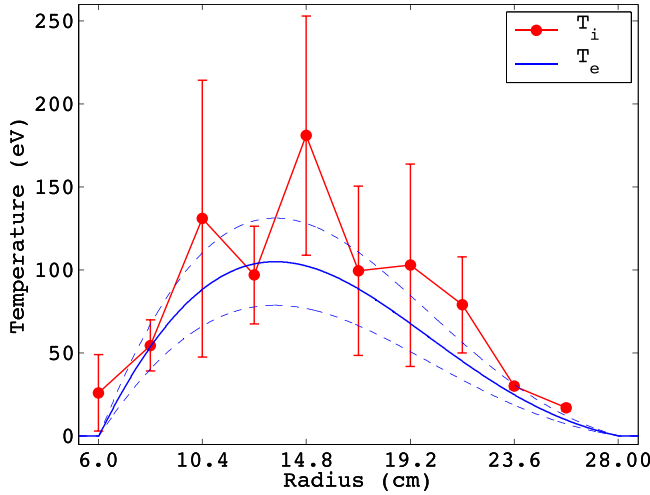


FIG. 6. Electron temperature profile which yields the best fit to the measured emission spectrum. The dashed lines represent the uncertainty in $T_e(r)$ that results from uncertainty in measuring the dynamic L_n . The ion temperature profile was measured using spectroscopy and is shown for comparison.

in order to shift the cyclotron resonances and the measurement and fitting process were repeated. In each case, the model accurately predicts the frequency at which the emission intensity peaks as well as selecting cone angles and temperature profiles, which vary by only a few percent. The consistency of these results gives us confidence that even in light of the uncertainties in measuring the dynamic L_n and the many simplifying assumption made, the code is able to capture the essential physics involved and provides a useful estimation of the electron temperature.

Combined measurements of the ion and electron temperatures allow us to estimate the energy confinement time, τ_E for a typical discharge. Here, we define τ_E to the total thermal and rotational energy divided by the total input power. The total thermal energy, averaged over 60 discharges is 2.44 ± 0.85 kJ, and the total kinetic energy is 1.00 ± 0.35 kJ. The only source of input power to the plasma is the radial electric current, which provides both plasma heating and rotation. Thus, the total input power is $P_{in} = I_P V_p$, where I_P and V_p are the current and voltage between the axial

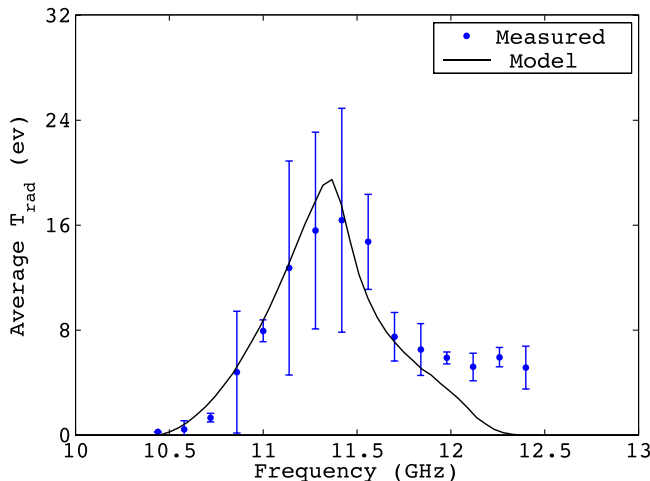


FIG. 7. The measured EBW spectrum compared with the predicted emission spectrum.

electrode and the vacuum vessel. The average input power in a typical discharge is 5.8 ± 0.42 MW, yielding an energy confinement time of 590 ± 160 μ s.

VI. POSSIBLE CONTRIBUTION OF HOT ELECTRONS

As a final point, we eliminate the possibility that the emission bursts may be related to a non-thermal population of hot electrons. Non-thermal emission from hot electrons is always a concern in a plasma generated by intense electric discharge, such as in MCX. Some fraction of the electrons may be accelerated to energies corresponding to the discharge voltage, leading to a population of hot electrons intermingled with a cold electron background. These hot electrons emit radiation at harmonics of the cyclotron frequency with much greater intensity than the cold electron background so that the emission spectrum is no longer a simple function of temperature. Because we observe radiation in intense bursts associated with an instability in the plasma, hot electrons are of particular concern. We are only concerned with electrons that have kinetic energy of several keV, as lower energy electrons will quickly thermalize. Electrons with keV energies produce X-ray photons from collisions with the walls of the chamber and with other charged particles in the plasma with X-ray photon energies up to electron energy.⁵ Thus, if a superthermal population of electrons is present in MCX, we would expect to observe X-ray emission with photon energies up to the discharge voltage, around 4 keV.

To this end, X-ray emission from the plasma was measured using a Princeton Instruments PIXIS-XO fast X-ray camera. UV light from the plasma was blocked from the camera using a thin Ni foil (0.2 μ m). To verify the functionality of the camera-filter system, X-rays were generated by setting up a continuous glow discharge between the central electrode and the vacuum vessel with the magnets turned off. In this arrangement the chamber is filled to 30 mTorr with hydrogen, and a continuous voltage that may be set from -1 to -3.5 kV applied between the core electrode and the vacuum vessel in the absence of a magnetic field. These discharges produced copious X-rays with energies up to the discharge voltage that were easily detected by the camera. Figure 8 shows a comparison between the X-ray emission from the rotating plasma

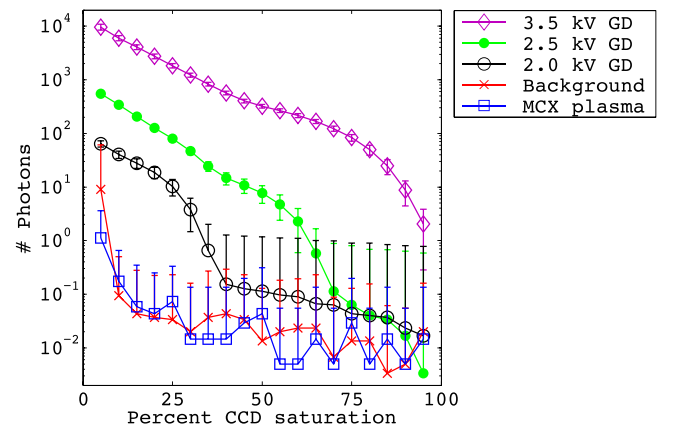


FIG. 8. Histogram of X-ray photons collected from the rotating plasma, background and three glow discharges with various discharge voltages. The percent CCD saturation serves as a proxy for photon energy.

gathered over 80 discharges compared to background and three glow discharges with discharge voltages from -2.0 to -3.5 kV. The rotating plasma X-ray generation is essentially the same as background, clearly showing that there is no detectable population of electrons with energies greater than 1 keV in the rotating plasma. Based on the absence of detectable X-ray emission, we conclude that there is no significant population of hot electrons within the plasma and that the observed radiation is thermal in origin.

VII. CONCLUSION

Microwave radiation consistent with electron Bernstein emission in the 2nd harmonic of the cyclotron frequency has been observed at the mid-plane of the MCX device. In the absence of detectable X-ray photons from the plasma, the EBW emission is considered to be thermal. An array of electrostatic probes has been successfully employed to measure the density gradient at the mode conversion layer. The B-X conversion efficiency is highly variable as a result of turbulence at the edge of the rotating plasma. The coupling efficiency can be improved with the use of a local limiter, but is at best only 20% on average. The emission serves as a temperature diagnostic, albeit with temporal resolution limited to about $10\ \mu\text{s}$ as only the average mode conversion efficiency can be measured at present. The radiation intensity, combined with measurements of the density gradient, indicates an average electron temperature around 80 eV, with a peak temperature that exceeds 100 eV in core of the rotating plasma.

ACKNOWLEDGMENTS

We gratefully thank Dr. John Rodgers for both the loan of vital equipment and many stimulating conversations. Work supported by the U.S. Department of Energy.

- ¹Y.-M. Huang and A. Hassam, *Phys. Rev. Lett.* **87**, 235002 (2001).
- ²R. F. Ellis, A. Case, R. Elton, J. Gosh, H. Griem, A. Hassam, R. Lunsford, S. Messer, and C. Teodorescu, *Phys. Plasmas* **12**, 055704 (2005).
- ³C. Teodorescu, R. Ellis, A. Case, C. Cothran, A. Hassam, R. Lunsford, and S. Messer, *Phys. Plasmas* **12**, 062106 (2005).
- ⁴W. C. Young, A. Hassam, C. Romero-Talamás, R. F. Ellis, and C. Teodorescu, *Phys. Plasmas* **18**, 112505 (2011).
- ⁵I. H. Hutchinson, *Principles of Plasma Diagnostics* (Cambridge University Press, Cambridge CB2 2RU, UK, 2002).
- ⁶J. Ghosh, R. C. Elton, H. R. Griem, A. Case, R. Ellis, A. Hassam, S. Messer, and C. Teodorescu, *Phys. Plasmas* **11**, 3813 (2004).
- ⁷H. Laqua and H. Hartfub, *Phys. Rev. Lett.* **81**, 2060 (1998).
- ⁸P. Chattopadhyay, J. Anderson, T. Biewer, D. Craig, C. Forest, R. Harvey, and A. Smirnov, *Phys. Plasmas* **9**, 752 (2002).
- ⁹B. Jones, P. Efthimion, G. Taylor, T. Munsat, J. R. Wilson, J. Hosea, R. Kaita, R. Majeski, and A. K. Ram, *Phys. Rev. Lett.* **90**, 165001 (2003).
- ¹⁰M. Bornatici, C. Maroli, and V. Petrillo, in "Heating in toroidal plasmas," in *Proceedings of the 3rd Joint Varenna-Grenoble International Symposium*, 1982, Vol. II.
- ¹¹A. K. Ram and S. D. Schultz, *Phys. Plasmas* **7**, 4084 (2000).
- ¹²I. U. Uzun-Kaymak, P. N. Guzdar, S. Choi, M. R. Clary, R. F. Ellis, A. B. Hassam, and C. Teodorescu, *Phys. Plasmas* **15**, 112308 (2008).
- ¹³I. U. Uzun-Kaymak, P. N. Guzdar, R. F. Ellis, A. B. Hassam, and C. Teodorescu, *Europhys. Lett.* **85**, 15001 (2009).
- ¹⁴S. Choi, P. N. Guzdar, A. Case, R. Ellis, A. B. Hassam, R. Lunsford, C. Teodorescu, and I. Uzun-Kaymak, *Phys. Plasmas* **15**, 042507 (2008).
- ¹⁵C. A. Romero-Talamás, R. C. Elton, W. Young, R. Reid, and R. F. Ellis, *Phys. Plasmas* **19**, 072501 (2012).